

Correction to the chiral magnetic effect from axial-vector interactionZhao Zhang^{1,*}¹*School of Mathematics and Physics, North China Electric Power University, Beijing 102206, China*
(Received 12 January 2012; published 19 June 2012)

The recent lattice calculation at finite axial chemical potential suggests that the induced current density of the chiral magnetic effect (CME) is somehow suppressed compared with the standard analytical formula. We show in a Nambu-Jona-Lasino-type model of QCD that such a suppression is a natural result when considering the influence of the attractive axial-vector interaction. We point out that the lattice result does not need to be quantitatively consistent with the analytical formula due to the chirality density-density correlation. We also investigate the nonperturbative effect of instanton molecules on the CME. Since an unconventional repulsive axial-vector interaction is induced, the CME will be enhanced significantly by the instanton-anti-instanton pairings. Such a prediction needs to be tested by more improved lattice simulations. We further demonstrate that the axial-vector interaction plays an important role on the $T - \mu_A$ phase diagram.

DOI: [10.1103/PhysRevD.85.114028](https://doi.org/10.1103/PhysRevD.85.114028)

PACS numbers: 12.38.Aw, 12.38.Mh

I. INTRODUCTION

The topological charge of gauge field theory is defined as

$$Q_T = \frac{g^2}{32\pi^2} \int d^4x \text{Tr}[F\tilde{F}], \quad (1)$$

where F and \tilde{F} refer to the field strength tensor and its dual, respectively. It is well-known that quantum chromodynamics (QCD) contains nontrivial gauge configurations carrying the topological charge with an integer number [1]. These configurations interpolate between the topologically different vacua of QCD characterized by different Chern-Simons numbers. For a long time the experimental evidence for the existence of the topological gluon configurations only comes indirectly from the meson spectrum [2].

Recently, the study of the chiral magnetic effect (CME) [3,4] has received much attentions since the topological configurations of QCD may be observed directly in the noncentral heavy-ion collisions. The essence of the CME is the chiral imbalance induced by the nonzero topological charge through the axial anomaly of QCD

$$(N_R - N_L)_{t=+\infty} - (N_R - N_L)_{t=-\infty} = -2Q_T, \quad (2)$$

where $N_R(N_L)$ denotes the quark number of the right-handed (left-handed) chirality in the chiral limit. Equation (2) indicates the chiral asymmetry is generated by the nonzero topological excitations. In a strong magnetic field which may be produced in the noncentral heavy-ion collisions, a net electric current will be induced along the direction of the magnetic field due to the chirality imbalance.

In order to study the effect of the chiral asymmetry, usually the axial chemical potential μ_A is introduced in a grand canonical ensemble [4]. The physical meaning of μ_A is the difference of the right- and left-handed quark

chemical potentials. This quantity can be identified as the time derivative of the θ angle of QCD, namely, $\mu_A = \partial_0\theta/2N_f$ [4]. In the presence of an external magnetic field B , the analytical expression of the induced electric current density for the CME at finite μ_A has been given in [4], which takes the form

$$j_{\text{em}} = CN_c N_f e^2 \mu_A B, \quad (3)$$

where $C = 1/2\pi^2$. Note that all quarks carrying the same electric charge is assumed in (3). Obviously, this equation explicitly breaks the \mathcal{P} and \mathcal{CP} symmetry.

Equation (3) indicates that the hot quark-gluon plasma is an ideal place to study the physics of \mathcal{P} - and \mathcal{CP} -odd excitations of QCD. First, the production probability of the configurations with nonzero winding numbers becomes higher since jumping over the potential barrier between distinct classical vacua is probable at high temperatures. The configurations responsible for such thermal transitions are called sphalerons [5,6] in QCD, which might occur at a copious rate at high temperature compared to the low-temperature tunneling by the instanton. Second, a strong magnetic field can be produced in noncentral heavy-ion collisions [3,7]. The study based on the UrQMD model [7] suggests that the eB produced at RHIC and LHC can be as large as $eB \approx 2m_\pi^2$ and $eB \approx 15m_\pi^2$, respectively.¹ So in a noncentral heavy-ion collision, the induced electric current may lead to an excess of the positive electric charge on one side of the reaction plane and the negative electric charge on the other. Such a charge separation effect may be observed experimentally. Recently, a conclusive observation of charge azimuthal correlation has been presented by

¹The magnetic field strength can be translated into the CGS system with the identity $m_\pi^2 \approx 10^{18}$ Gauss, where $m_\pi = 140$ MeV.

*zhaozhang@pku.org.cn

the Star collaboration [8] which may result from the CME with local \mathcal{P} and \mathcal{CP} violation.

Theoretically, the investigation of the CME has been performed recently in the Lattice QCD simulation by introducing a finite μ_A [9]. The advantage of the lattice simulation at finite axial chemical potential is that there is no sign problem comparing with the case at finite baryon chemical potential. In this study, the CME described by Eq. (3) has been confirmed qualitatively. But at the quantitative level, the obtained electric current density is significantly suppressed [9] compared to the analytical formula (3). The further study at the quenched level of QCD suggests that the lattice data are sensitive to the lattice spacing [10] and the obtained data increase significantly compared to the ones in [9]. However, the deviation of the new lattice data from the analytical formula is still sizable even some systematic errors have been taken into account [10].

The suppression of the lattice data may stem from some errors of the lattice simulation and/or the nonperturbative effects of QCD. Accordingly, besides taking more improved lattice calculations, physically understanding the current lattice result through other methods of QCD is very important and necessary. On the other hand, due to the limitation of the lattice calculation, investigating the nonperturbative corrections and making new predictions on the CME are also very required by using the effective theories or models of QCD.

The purpose of this paper has two aspects: First, we will try to disclose the possible mechanism for the deviation of the present lattice data from the analytical result by taking into account some QCD corrections; second, we will explore the nonperturbative influence of the instanton molecules on the CME and make some predictions. Note that both aspects are closely related to the effective four-quark interaction in the axial-vector channel, where the chirality density-density correlation plays an important role.

The paper is organized as follows: In Sec. II, we give the effective quark interactions of QCD for $T > T_c$. In Sec. III, we present the correction to the CME from the axial-vector interaction. Section IV is devoted to the numerical results and related discussions. The last section is the summary and conclusion.

II. EFFECTIVE QUARK INTERACTIONS FOR $T > T_c$

The experimental data of RHIC suggests that strongly coupled quark-gluon plasma (sQGP) is formed for $T > T_c$, which exhibits the behavior of a perfect fluid. Now it is widely believed that the nonperturbative QCD still plays very important roles on the hot quark-gluon plasma up to $2-3T_c$. Since the chiral magnetic effect may be observed directly in heavy-ion collisions, one naturally expects that the role of the nonperturbative aspects of QCD on the CME should be quite remarkable. One of the possible

nonperturbative effects may arise from the instanton-anti-instanton ($I\bar{I}$) molecules at finite temperature near T_c .

As a major component of the QCD vacuum, the instantons can produce the quark condensate, the low-lying hadron state and other nonperturbative features of QCD, according to the interacting instanton liquid model [11]. At zero and low temperatures, the instanton ensemble is in a random liquid state which is responsible for the spontaneous chiral symmetry breaking and the axial anomaly. Naively, one would expect that the instantons might give a little contribution to the CME due to their significant suppression at high temperature.

However, it has been suggested that the hot chiral transition is not driven by the vanishing of the instantons and anti-instantons but by their rearrangement around T_c [12–14]. Namely, when approaching to T_c from below, the random instantons and anti-instantons are paired up into the ordered $I\bar{I}$ molecules. This picture implies that the instantons still keep sizable density near T_c with the molecular forms. Moreover, a recent investigation indicates that the $I\bar{I}$ molecules can even survive up to $\sim 5T_c$ [15].

The rearrangement picture indicates that the nonperturbative effects induced by the instanton configurations will persist into the high temperature region. In the chiral symmetric phase, the interacting $I\bar{I}$ molecules can be regarded as one of the possible mechanisms responsible for the sQGP formed in $T_c < T < 2 \sim 3T_c$ [16]. So even though the chiral restoration is one of the necessary conditions for the appearance of the electric current j_{em} , the instantons may still exert important influence on the chiral magnetic effect via the molecular forms.

It is well-known that the random instanton configurations can lead to the famous 't Hooft interactions among quarks with different flavors

$$\mathcal{L}_{t\text{Hooft}} \sim \prod_f (\bar{\psi} \phi_0)(\bar{\phi}_0 \psi), \quad (4)$$

which explicitly breaks the $U_A(1)$ symmetry due to the axial anomaly. Similarly, the ordered $I\bar{I}$ molecules also result in effective quark interactions, but only with the four-fermion coupling forms. For the two-flavor case, the Fierz-invariant quark interactions induced by $I\bar{I}$ molecules has been derived in [14] with the form

$$\begin{aligned} \mathcal{L}_{\text{molsym}} = G \left\{ \frac{2}{N_c^2} \sum_{a=0}^3 [(\bar{\psi} \tau^a \psi)^2 - (\bar{\psi} \tau^a \gamma_5 \psi)^2] \right. \\ \left. + \frac{2}{N_c^2} (\bar{\psi} \gamma_\mu \gamma_5 \psi)^2 - \frac{1}{2N_c^2} \sum_{a=0}^3 [(\bar{\psi} \tau^a \gamma_\mu \psi)^2 \right. \\ \left. + (\bar{\psi} \tau^a \gamma_\mu \gamma_5 \psi)^2] \right\} + \mathcal{L}_8, \quad (5) \end{aligned}$$

where τ^0 and $\vec{\tau}$ are unit and Pauli matrices in flavor space, respectively, and G is the coupling constant. The \mathcal{L}_8 in (5) refers the quark interactions in the color octet channel. In

the $I\bar{I}$ molecular picture, it is expected that the dominant quark interactions for $T > T_c$ are the molecular ones rather than the 't Hooft interactions [13–16].² Different from (4), the Lagrangian (5) respects not only the $SU_V(2) \otimes SU_A(2) \otimes U_B(1)$ symmetry, but also the $U_A(1)$ symmetry. This is because the $I\bar{I}$ pair gives vanishing topological charges [14].

Note that the most general Fierz-invariant form for the four-quark interactions under the invariance of $SU_V(2) \otimes SU_A(2) \otimes U_B(1) \otimes U_A(1)$ symmetry including both the scalar (pseudoscalar) and vector (axial-vector) currents is

$$\begin{aligned} \mathcal{L}_{\text{general}}^{(4)} = & \frac{1}{2}G_1 \sum_{a=0}^3 [(\bar{\psi}\tau^a\psi)^2 + (\bar{\psi}\tau^a i\gamma_5\psi)^2] \\ & - \frac{1}{2}G_2 \sum_{a=0}^3 [(\bar{\psi}\tau^a\gamma_\mu\psi)^2 + (\bar{\psi}\tau^a\gamma_\mu\gamma_5\psi)^2] \\ & - \frac{1}{2}G_3 [(\bar{\psi}\tau^0\gamma_\mu\psi)^2 + (\bar{\psi}\tau^0\gamma_\mu\gamma_5\psi)^2] \\ & - \frac{1}{2}G_4 [(\bar{\psi}\tau^0\gamma_\mu\psi)^2 - (\bar{\psi}\tau^0\gamma_\mu\gamma_5\psi)^2] + \mathcal{L}_8^{(4)}, \end{aligned} \quad (6)$$

where G_i are four independent coupling constants [17]. Comparing (5) with (6), one can find that the interacting $I\bar{I}$ molecule model (IIMM) predicts these coupling constants with

$$G_1 = \frac{4}{N_c^2}G, \quad G_2 = \frac{1}{N_c^2}G, \quad G_4 = -G_3 = \frac{2}{N_c^2}G, \quad (7)$$

which are all dependent on the only parameter G . We shall show below that nonzero G_2 and $G_{3(4)}$ give nontrivial contributions to the induced current j_{em} for the CME.

We stress that even though we are very interested in the possible nonperturbative influence of the instantons on the CME, we do not limit our study within the only formalism (5), which is just a special case of (6). Without loss of generality, we will assume that the Lagrangian density with the four-quark interactions (6) works for $T_c < T < 2 \sim 3T_c$. This Lagrangian can be regarded as an extension of the traditional Nambu-Jona-Lasino (NJL) model of QCD (In the next section, the degree of freedom of the Polyakov loop is also included).

For the physics related to the CME, we are particularly interested in the effective four-quark interactions in the vector isospin-scalar and axial-vector isospin-scalar channels

$$\mathcal{L}_{VA} = -G_V(\bar{\psi}\gamma_\mu\psi)^2 - G_A(\bar{\psi}\gamma_\mu\gamma_5\psi)^2, \quad (8)$$

²Note that the 't Hooft-type interactions might also survive in the $T > T_c$ region according to [15]. Such interactions should have little influence on the CME since the electric current only appears in the chirally symmetric phase.

which appears in both (5) and (6). The significance of \mathcal{L}_{VA} to the CME is attributed to the appearance of two special vacuum expectation values (VEVs) in the chirally asymmetric system under the influence of an external magnetic field B , namely, $j_z = \langle \bar{\psi}\gamma^3\psi \rangle$ and $n_A = \langle \bar{\psi}\gamma_0\gamma_5\psi \rangle$ [4]. The former is the VEV of the vector current $\bar{\psi}\gamma^\mu\psi$ along the direction of B and the latter the chiral charge density conjugate to μ_A . As a consequence, the chiral magnetic effect might be sensitive to the couplings G_V and G_A in (8).

The prediction of the IIMM gives

$$G_V = \frac{G_2}{2} = \frac{G}{2N_c^2}, \quad G_A = 2G_4 + \frac{G_2}{2} = -3\frac{G}{2N_c^2}. \quad (9)$$

Equation (9) indicates two unconventional points induced by the $I\bar{I}$ molecules: (1) The vector interaction is attractive while the negative G_A implies that the axial-vector interaction is repulsive; (2) The magnitude of G_A is three times that of G_V (For the totally polarized case, the coupling G_A in the temporal direction is even 12 times that of G_V [14]).

This is quite different from the conventional four-quark interactions derived from the Fierz transformation of the colored quark-antiquark current-current interaction

$$\mathcal{L}_{\text{OGEA}} = g(\bar{\psi}\gamma_\mu\lambda_c^a\psi)^2, \quad (10)$$

which arises from the one gluon exchange approximation (OGEA) of QCD. In the OGEA, both G_V and G_A are positive with

$$G_V = G_A = \frac{G_S}{2}, \quad (11)$$

where G_S is the coupling constant in the scalar isoscalar channel.

Note that it is very likely that the effective quark interactions stemming from the OGEA can persist into the nonperturbative region of QCD with relatively strong couplings. A well-known example in the literature is the global color model (GCM) of QCD, which is based on the non-local colored quark-antiquark current-current interaction

$$\mathcal{L}_{\text{GCM}}(x, y) = g(x - y)\bar{\psi}(x)\gamma_\mu\lambda_c^a\psi(x)\bar{\psi}(y)\gamma^\mu\lambda_c^a\psi(y), \quad (12)$$

where $g(x - y)$ is a function of the strong coupling [18]. This model can successfully describe the low-lying hadrons [19] and give reasonable QCD condensates in the vacuum and at finite temperature and density [20].

Since the axial-vector interaction may be repulsive (as in the IIMM) or attractive (as in the OGEA or GCM), we will treat the coupling G_A in (8) as a free parameter. The realistic G_A may include contributions from both the $I\bar{I}$ molecules and the OGEA, which should depend on the temperature in general. On the other hand, since the vector interaction is attractive in both the IIMM and GCM, we only consider the positive G_V in the following.

III. CORRECTION TO THE CME FROM AXIAL-VECTOR INTERACTION

Working at the mean field level, the Lagrangian (8) can be rewritten as

$$\mathcal{L}_{VA}^{\text{MF}} = G_A n_A^2 - 2G_A n_A \bar{\psi} \gamma_0 \gamma_5 \psi - G_V j^z + 2G_V j^z \bar{\psi} \gamma^3 \psi. \quad (13)$$

We can read two nontrivial points from Eq. (13). First, both squared terms of the condensates j^z and n_A give contributions to the thermodynamical potential. Second, the four-quark interactions in the axial-vector and vector channels lead to a dynamical axial chemical potential $\mu'_A = -2G_A n_A$, and an effective gauge field $A^z = -2G_V j^z$ along the direction of B , respectively. Note that both points are not taken into account in [4] to derive the analytical formula for the CME current.

To investigate the dynamical influence of \mathcal{L}_{VA} on the CME, we add the kinetic Lagrangian for free-interacting quarks, namely, $\mathcal{L}_{\text{kin}} = \bar{\psi}(i\gamma_\mu \partial_\mu + \mu_A \gamma^0 \gamma^5)\psi$ to the Lagrangian (6). We will work in the chiral limit throughout this paper. To describe the confinement-deconfinement transition of QCD, we also include the dynamics of the Polyakov loop, the action of which the pure gauge theory denotes as \mathcal{U} . Our model can be looked as the Polyakov-loop-enhanced IIMM but with a varying axial-vector coupling G_A . In form, it is very similar to the so-called two-flavor Polyakov-loop extended Nambu-Jona-Lasino model [21].

One then gets the mean field thermodynamical potential

$$\begin{aligned} \Omega = & \mathcal{U} + G_S \sigma^2 + G_V j^z{}^2 - G_A n_A^2 \\ & - N_c \sum_{f=u,d} \frac{|q_f B|}{2\pi} \sum_{s,k} \alpha_{sk} \int_{-\infty}^{\infty} \frac{dp_z}{2\pi} f_\Lambda^2 \omega_s(p) \\ & - 2T \sum_{f=u,d} \frac{|q_f B|}{2\pi} \sum_{s,k} \alpha_{sk} \\ & \times \int_{-\infty}^{\infty} \frac{dp_z}{2\pi} \ln(1 + 3\Phi e^{-\beta\omega_s} + 3\bar{\Phi} e^{-2\beta\omega_s} + e^{-3\beta\omega_s}), \end{aligned} \quad (14)$$

where

$$\alpha_{sk} = \begin{cases} \delta_{s,+1} & \text{for } k = 0, eB > 0, \\ \delta_{s,-1} & \text{for } k = 0, eB < 0, \\ 1 & \text{for } k \neq 0, \end{cases} \quad (15)$$

and f_Λ is the UV regulator function. Φ and $\bar{\Phi}$ in (14) correspond to the normalized traced Polyakov loop and its Hermitean conjugate, respectively. In (15), s refers to the spin and k denotes the Landau level. The dispersion relations of the quasiparticles derived from the eigenvalues of the Dirac operator take the form

$$\omega_s^2 = M^2 + [|\mathbf{p}| + s\tilde{\mu}_A \text{sgn}(p_z)]^2, \quad (16)$$

where

$$|\mathbf{p}|^2 = |\tilde{p}^z|^2 + 2|q_f B|k \quad (17)$$

and q_f stands for the electric charge for f (u or d) quark. In the above equations, $\tilde{\mu}_A$ and \tilde{p}^z refer to the effective axial chemical potential and the modified momentum along \mathbf{B} , respectively, namely

$$\tilde{\mu}_A = \mu_A + \mu'_A = \mu_A - 2G_A n_A, \quad (18)$$

$$\tilde{p}^z = p^z + A^z = p^z - 2G_V j^z. \quad (19)$$

The current j^z , the chirality density n_A , the quark condensate³ σ , and the VEV of the Polyakov loop Φ can be determined self-consistently by solving the saddle point equations:

$$\frac{\partial \Omega}{\partial n_A} = 0, \quad \frac{\partial \Omega}{\partial j^z} = 0, \quad \frac{\partial \Omega}{\partial \sigma} = 0, \quad \frac{\partial \Omega}{\partial \Phi} = 0. \quad (20)$$

Note that the influence of G_V on the CME has been investigated in [22], where only the vector interaction is introduced phenomenologically. The main conclusion is that G_V may lead to a dielectric correction to the CME current density

$$j = \frac{1}{2\pi^2(1 + 2G_V \mathcal{C}_R)} \cdot N_c N_f e \mu_A B, \quad (21)$$

where $\mathcal{C}_R = \frac{|eB|}{2\pi^2}$ [22]. When including the axial-vector interaction, the dispersion relation (16) suggests that Eq. (21) will be further modified as

$$j = \frac{1}{2\pi^2(1 + 2G_V \mathcal{C}_R)} \cdot N_c N_f e \tilde{\mu}_A B. \quad (22)$$

However, a subtlety on the calculation of the polarization tensor or susceptibility in [22] has been pointed out by Kenji Fukushima [23]: According to Eqs. (8-10) in [23], the quantity \mathcal{C}_R should be zero since the corresponding static susceptibility $\Pi^{33}(q^0 = 0, \vec{q} \rightarrow 0)$ is always vanishing. This implies that the vector interaction does not give any correction to the CME. Actually, this point is also consistent with the Nielsen-Ninomiya's argument [24] which is only based on the nonrenormalization of triangle anomalies and the energy conservation. As shown in Eq. (21) [or Eq. (22)], the nonzero \mathcal{C}_R will lead to a modification of the coefficient before $\mu_A B$ (or $\tilde{\mu}_A B$ in our case). Nevertheless, the argument proposed by Nielsen and Ninomiya [24] does not support the coefficient receiving any correction. This is because such a coefficient is determined by the nonrenormalization of triangle anomalies, which is known exactly due to the topological

³Strictly speaking, there should be two chiral order parameters in the chiral limit since $\langle \bar{\psi}_L \psi_R \rangle \neq \langle \bar{\psi}_R \psi_L \rangle$ for nonzero μ_A .

nature of anomalies (for more details of this argument, see the first part of Sec. III in [4]).

In light of this, the correct formula for the current density should be

$$j = \frac{1}{2\pi^2} N_c N_f e \tilde{\mu}_A B, \quad (23)$$

rather than Eq. (22) when considering the axial-vector interaction. We note that, unlike Eqs. (21) and (22), Eq. (23) does not contradict Nielsen-Ninomiya's argument. This is because the energy required to remove a particle from the left-handed Fermi surface and add it to the right-handed Fermi surface is no longer $2\mu_A$ but $2\tilde{\mu}_A$ due to the influence of the axial-vector interaction. In fact, Eq. (23) will be obtained naturally if we take the same method as part A of Sec. 3 in [4] but with the replacement of μ_A with $\tilde{\mu}_A$.

In the following, we will ignore the vector interaction and only consider the effect of the axial-vector interaction on the CME. Using the method

$$j_{\text{em}} = - \left. \frac{\partial \Omega}{\partial A_3} \right|_{A_3=0} \quad (24)$$

and the replacement

$$\frac{\partial}{\partial A^z} \rightarrow q_f \frac{d}{dp_z}, \quad (25)$$

one can get the integral expression for the calculation of the electric current density in the two-flavor case

$$j_{\text{em}} = N_c \sum_{f=u,d} q_f \frac{|q_f B|}{2\pi} \times \sum_{s,k} \alpha_{ks} \int_{-\infty}^{\infty} \frac{dp_z}{2\pi} \frac{d}{dp_z} [f_{\Lambda}^2 \omega_s(p) + \dots]. \quad (26)$$

As the case of zero G_A , only the lowest Landau level (LLL) gives a nonvanishing contribution in (26). Ignoring the correction from G_V , the induced electric current density j_{em} for the two-flavor case under the influence of G_A becomes

$$j_{\text{em}} = N_c \sum_{f=u,d} \frac{q_f^2 \tilde{\mu}_A B}{2\pi^2} = \frac{5\tilde{\mu}_A e^2 B}{6\pi^2}. \quad (27)$$

As it should be, Eq. (27) indicates that the induced electric current density is ultraviolet finite.

Unlike the analytical formula (3), the chirality density n_A appears directly in Eq. (27). This density can be obtained self-consistently by

$$\frac{\partial \Omega}{\partial n_A} = 0 \rightarrow n_A = - \frac{\partial \Omega}{\partial \mu_A} = - \frac{\partial \Omega}{\partial \tilde{\mu}_A}, \quad (28)$$

according to (18). This equation is similar to the determination of the baryon number density at finite μ when considering the vector interaction in the NJL-type model

[25]. We note that even though the formula (27) is obtained from the LLL integration, it doesn't mean that j_{em} only depends on the LLL for nonzero G_A since the high Landau levels also give contributions to the chirality density n_A .

The modified expression of j_{em} implies that the induced electric current density under the influence of the axial-vector interaction may deviate from the analytical result in the following aspects. First, the current density j_{em} is no longer directly proportional to the axial chemical potential μ_A and the magnetic field B . The reason is that in general, the dynamical chemical potential μ'_A doesn't linearly depend on μ_A and B . Second, μ'_A is T dependent (since G_A and n_A are both T dependent), so the current density j_{em} also depends on the temperature. Third, the IIMM predicts that the CME will be enhanced significantly: (1) μ'_A has the same sign as μ_A because of the negative G_A ; (2) μ'_A may be sizable since G_A is strong as G_S . In contrast, the OGEA (or GCM) predicts that the CME will be weakened by the attractive axial-vector interaction compared to the analytical result.

IV. NUMERICAL RESULTS AND DISCUSSIONS

In this section, we provide numerical results for the influence of the axial-vector interaction on the chirally imbalanced matter in a constant magnetic field. The coupling G_S , the UV regulator function $f_{\Lambda}(p)$ and the Polyakov-loop model \mathcal{U} in (14) are all adopted from [26], in which the Polyakov-loop extended Nambu-Jona-Lasino model was used to study the CME. The model parameters of the NJL part are fitted by reproducing the pion decay constant and the quark condensate in the vacuum. The T_c for vanishing μ_A , B , and G_A is ~ 228 MeV with the influence of the Polyakov-loop dynamics [26].

A. Effect of axial-vector interaction on the chiral magnetic effect

We will focus on the variation of the ratio

$$R = j_{\text{em}}/j_{\text{em}}(G_A = 0) = \tilde{\mu}_A/\mu_A \quad (29)$$

with the impact of the coupling G_A . The quantity $R = R(G_A, T, \mu_A, B)$ corresponds to the ratio $C/2\pi^2$, which is the focus of the recent lattice QCD calculations [9,10]. The deviation of R from the unity reflects the influence of the axial-vector interaction on the CME compared to the analytical formula.

In Fig. 1, we first show the dependence of R on the coupling G_A for different μ_A with fixed $eB = 4 \times 10^{18}$ Gauss and $T = 230$ MeV. The density of $I\bar{I}$ molecules might be sizable at this temperature since it is just slightly greater than T_c (The catalytic effect of the magnetic field on the chiral symmetry breaking can be ignored for such an eB [26]). We see that R decreases monotonically with increasing G_A . The electric current density is enhanced by $G_A < 0$ and weakened by $G_A > 0$. Its deviation from the analytical value is quite

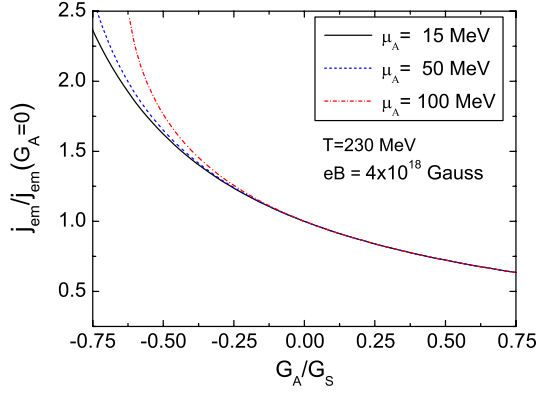


FIG. 1 (color online). The ratio of j_{em} to $j_{em}(G_A = 0)$ as a function of G_A for different μ_A . The eB and T are fixed as 4×10^{18} Gauss and 230 MeV, respectively.

significant: For the moderate coupling $G_A/G_S = -0.5$ (0.5), the electric current density increases (decreases) by ~ 62 (27) percent at $\mu_A = 15$ MeV; While for the strong coupling $G_A/G_S = -0.75$ (0.75), the electric current density increases (decreases) by ~ 140 (34) percent at the same μ_A . This is in contrast to the minor modification of j_{em} caused by the vector interaction [22].

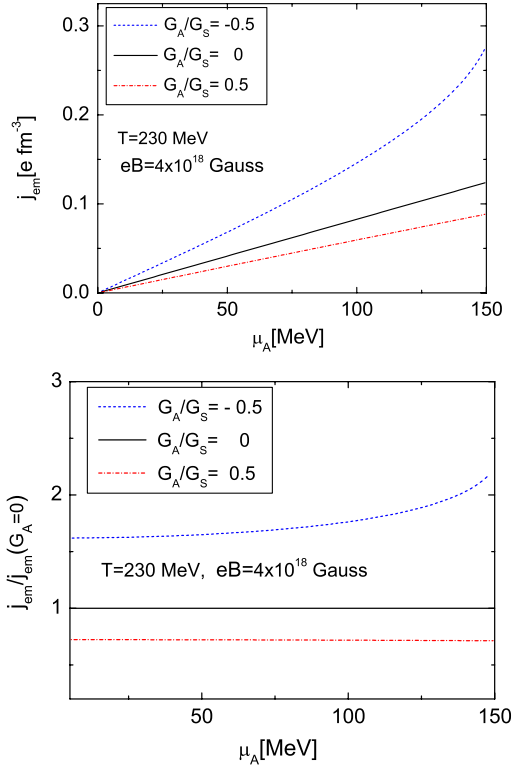


FIG. 2 (color online). Upper panel: The current j_{em} as a function of μ_A for different G_A . Lower panel: The ratio of j_{em} to $j_{em}(G_A = 0)$ as a function of μ_A for different G_A . The eB and T are fixed as 4×10^{18} Gauss and 230 MeV, respectively.

Figure 2 shows the electric current density j_{em} and the ratio R as functions of μ_A for different G_A , where the same T and B are used as in Fig. 1. For $G_A = -0.5$, the upper panel indicates that the electric current density is nearly proportional to μ_A in the small μ_A region, but its deviation from the linear behavior becomes more and more significant with increasing μ_A . Different from this, the electric current density almost linearly depends on μ_A up to the moderate μ_A region for $G_A = 0.5$. These features are demonstrated more clearly in the lower panel of Fig. 2: The ratio R monotonically increases with μ_A for $G_A = -0.5$ while almost remains as a constant for $G_A = 0.5$. The same information can be read from Fig. 1. This is because the chirality density rises more rapidly with growing μ_A for the repulsive axial-vector interaction.

The dependence of R on the temperature with $\mu_A = 15$ MeV and $eB = 2 \times 10^{18}$ Gauss is displayed in Fig. 3. For $G_A < 0$, the ratio R monotonically increases with increasing T and its deviation from one becomes huge for the strong coupling. For $G_A > 0$, the ratio R decreases relatively slowly with growing T for both the moderate and strong couplings. Though the change of R by T is not so significant as $G_A < 0$, the ratio R still decreases by ~ 10 (15) percent from $\sim T_c$ to $\sim 1.1T_c$ for $G_A/G_S = 0.5$ (1). Hence, the temperature has a noticeable effect on the induced current. The reason is that the density n_A is a monotonically increasing function of T , as reported in [26].

Figure 4 indicates that the ratio R is not so sensitive to the external magnetic field but still slowly rises (drops) with eB for $G_A < 0$ ($G_A > 0$). This is because that the chirality density is enhanced by the magnetic field through the increase of the thermodynamical potential [4]. Note that such a tendency will slow down or cease for large enough B since its catalytic effect on the chiral symmetry breaking: The enhancement of the chiral condensate by the magnetic field will suppress the chirality density.

Figures 1–4 imply that the chirality density-density correlation has an important impact on the chiral magnetic

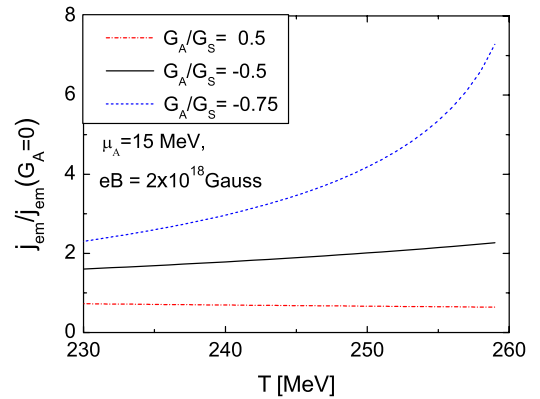


FIG. 3 (color online). The ratio of j_{em} to $j_{em}(G_A = 0)$ as a function of T for different G_A . The μ_A and eB are fixed as 15 MeV and 2×10^{18} Gauss, respectively.

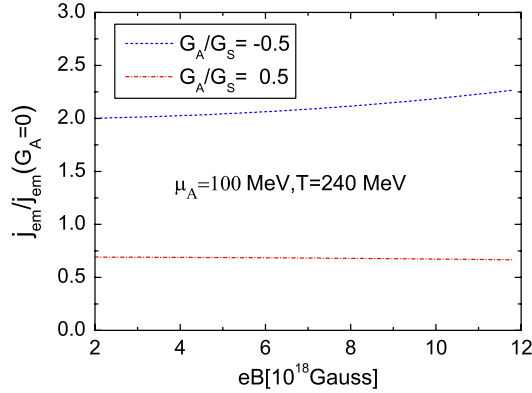


FIG. 4 (color online). The ratio of j_{em} to $j_{\text{em}}(G_A = 0)$ as a function of eB for different G_A . The μ_A and T are fixed as 100 MeV and 240 MeV, respectively.

effect, no matter the axial-vector interaction arises from the $I\bar{I}$ pairings, the OGEA, or the GCM. The ratio R can deviate significantly from the unity under the combined effects of G_A , μ_A , T , and B . The deviation may be positive or negative which depends on the sign of G_A . This contrasts with the role of G_V on the CME: It only affects the CME obviously when the magnetic field B is very large [22]; Its correction to the CME has nothing to do with μ_A and T .

Let us compare our results with the recent lattice QCD data. In [9], the CME was qualitatively confirmed by the lattice simulation via introducing a finite μ_A . However, the obtained coefficient C is around 0.013, which is far less than the analytical value $1/2\pi^2 \simeq 0.05$. The further study using the quenched simulation suggests that the suppression is sensitive to the lattice spacing [10]. The new lattice coefficient C is roughly in the range 0.02–0.03 [10], which increases greatly compared to the former results. However, it still much less than the standard analytical value. Moreover, another new point in [10] is that the coefficient C might be dependent on the temperature.

Regardless of the possible errors in [10], we stress that the current lattice data are quite natural when considering the effect of the attractive axial-vector interaction: (i) According to (27), the induced electric current is proportional to the effective axial chemical potential $\tilde{\mu}_A$, which may be suppressed significantly compared to μ_A by the positive G_A . As demonstrated in Figs. 1–4, the suppression is really remarkable for the moderate and strong couplings. So the reduction of $\tilde{\mu}_A$ by the attractive axial-vector interaction can explain why the lattice data of the induced electric current are much less than the analytical value. Let us make a rough comparison. According to Fig. 7 in [10], the lattice ratio $C/2\pi^2$ is located in 0.4–0.6 for $T \sim 1.1T_c$ ($T_c \sim 270$ MeV). Our numerical results shown in Fig. 3 suggest that the ratio R is in the range of 0.5–0.65 for $T \sim 1.1T_c$ ($T_c \sim 230$ MeV) if G_A/G_S varies from 1 to 0.5. We see that the lattice data are quite consistent with our results if the axial-vector interaction is

attractive and strong enough. (ii) The lattice data suggest that the coefficient C or the ratio $C/2\pi^2$ is insensitive to μ_A and eB . This feature is also in agreement with our results for the attractive axial-vector interaction, as shown in Figs. 2 and 4. (iii) One set of data ($\beta = 5.90$ with $N_t = 4, 6, 12$) in Fig. 7 of [10] indicates that the coefficient C decreases with growing T . The author has argued that such a behavior might be a lattice artifact. However, that the induced current density j_{em} may be suppressed by T can be well interpreted by the attractive coupling G_A as demonstrated in Fig. 3. According to Fig. 7 of [10], the ratio $C/2\pi^2$ decreases from ~ 0.53 to ~ 0.32 when increasing T from 317 MeV to 475 MeV; Or in other words, the ratio $C/2\pi^2$ decreases roughly by ~ 0.04 per $0.1T_c$. This is not so far away from the decline rate ~ 0.07 per $0.1T_c$ for $G_A/G_S = 0.5$, as indicated in Fig. 3.⁴ So to judge whether the coefficient C is sensitive to the temperature or not needs more detailed lattice investigation.

On the contrary, the IIMM predicts that the CME current or the coefficient C will be enhanced by the $I\bar{I}$ molecules. Clearly, this prediction deviates distinctly from the present lattice data. This might suggest that the dominant axial-vector interaction for $T > T_c$ is coming from the OGEA. Nevertheless, the current lattice simulation is still rough and far from conclusive (at least at the quantitative level). First, the fact that the current lattice data are sensitive to the lattice spacing [10] suggests that the continuum limit is very important for quantitatively understanding the chiral magnetic effect. Second, the main simulations in [10] are still at the quenched level while the discretization error of the fermion action is larger than that of the gauge action. Therefore, more improved quantitative lattice investigation will shed light on the role of the $I\bar{I}$ molecules on the chiral magnetic effect.

In any case, we stress that, due to the contribution of the dynamical axial chemical potential, the lattice result of the induced current for a finite μ_A doesn't need to be quantitatively consistent with the analytical formula. If there are no other QCD modifications, the coefficient C or the ratio R should be greater (less) than the standard analytical value for $G_A < 0$ ($G_A > 0$).

B. Effect of axial-vector interaction on the $T - \mu_A$ phase diagram

The chiral tricritical point (TCP) on the $T - \mu_A$ phase diagram has been found in [26], which locates at the relatively larger μ_A region (in the chiral limit for vanishing quark number density). The TCP is also confirmed in the linear sigma model, whose location is very close to the T axis [27]. These studies show that the $T - \mu_A$ phase diagram is somehow similar to the $T - \mu$ phase diagram of QCD.

⁴In the realistic case, the coefficient C should change more mildly since the coupling G_A becomes weaker with increasing T .

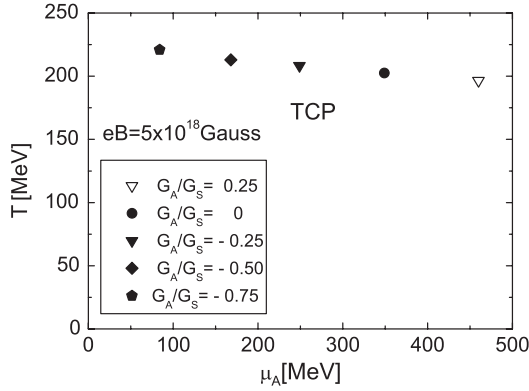


FIG. 5. The locations of the chiral TCP in the $T - \mu_A$ plane for different G_A .

Here we will demonstrate the role of the axial-vector interaction on the $T - \mu_A$ phase diagram. We are particularly interested in its influence on the TCP. In Fig. 5, we show the locations of the TCP for different axial-vector interactions. We see that the TCP is quite sensitive to the axial-vector coupling. The negative G_A shifts the TCP towards the smaller μ_A region while the positive G_A moves it towards the larger μ_A area. This implies that the first-order chiral transition is strengthened by the repulsive axial-vector interaction induced by $I\bar{I}$ molecules while weakened by the attractive axial-vector interaction stemming from the OGEA.

It is well-known that the attractive vector interaction can soften the chiral transition and move the critical point (CP) towards the larger μ area via generating a dynamical quark chemical potential [25,28]. Especially, when taking into account the two-flavor color superconductivity, the vector interaction combined with the charge-neutrality constraint and/or the axial anomaly can even lead to multiple chiral critical points [29].⁵ We observe from Fig. 5 that the attractive axial-vector interaction at finite μ_A has a similar influence on the chiral phase transition as the vector interaction does at finite μ .

However, in the instanton molecule model, the axial-vector interaction at finite μ_A and the vector interaction at finite μ have opposite effects on the chiral transition. Since the induced G_A and G_V have different signs, the chiral transition will be strengthened (softened) at finite μ_A (μ). In addition, the influence of the axial-vector interaction on the chiral transition at finite μ_A could be more remarkable since the coupling G_A is much stronger than G_V in the instanton molecule picture.

Locating the CP on the $T - \mu$ phase diagram is a focus of the current studies on the QCD phase transition and

⁵The new critical point might also appear through the interplay between the chiral condensates and the diquark condensates in the color-flavor-locking phase in the context of the axial anomaly [30].

heavy-ion collisions. So far, the location and even the existence of the CP is still under debate. Since there is no sign problem at finite μ_A , it is very interesting to explore the $T - \mu_A$ phase diagram of the chirally imbalanced matter and locate the TCP by means of the lattice simulation. Such an investigation may provide useful information on the true QCD phase transition. Moreover, studying the $T - \mu_A$ phase diagram through lattice QCD may shed light on the nonperturbative features of sQGP. For example, we can test the instanton molecule picture of QCD by investigating the $T - \mu_A$ phase diagram.

V. SUMMARY AND CONCLUSION

In this article, we have first investigated the influence of the axial-vector interaction on the chiral magnetic effect by introducing an axial chemical potential μ_A . Such an interaction can be induced by the instanton molecules or derived from the one gluon exchange approximation of QCD. In the presence of a finite chirality density n_A , a dynamical axial chemical potential μ'_A is generated through the density-density correlation. We derived that the induced electric current density j_{em} in an external magnetic field B linearly depends on the effective axial chemical potential $\tilde{\mu}_A$ which includes the contribution of μ'_A . Accordingly, the obtained j_{em} deviates from the standard analytical formula and explicitly depends on the chirality density n_A . In general, the deviation relies on the axial-vector coupling G_A , the axial chemical potential μ_A , the temperature T , and the magnetic field B .

For $G_A > 0$ from the one gluon exchange approximation, the induced current density can be significantly suppressed comparing with the analytical value. We also find that the ratio $R = j_{em}/j_{em}(G_A = 0)$ is insensitive to the axial chemical potential and the magnetic field but decreases with increasing temperature if $G_A > 0$. These features are quite consistent with the recent lattice results at finite μ_A . Hence, the suppression of the lattice data compared with the analytical formula can be attributed to the influence of the attractive axial-vector interaction of QCD. Actually, it is very likely that the deviation of the lattice result originates from the difference between μ_A and $\tilde{\mu}_A$. The reason is that Nielsen-Ninomiya's argument does not support the renormalization of CME if μ_A is not shifted dynamically.

On the contrary, an unconventional prediction from the instanton molecule model is that the axial-vector interaction is repulsive with $G_A < 0$ and is much stronger than the vector interaction. As a consequence, the chiral magnetic effect will be enhanced significantly by the instanton molecules near T_c . In such a picture, the ratio $j_{em}/j_{em}(G_A = 0)$ increases with both μ_A and T . These features deviate obviously from the current lattice results. Since the present lattice simulation at finite μ_A is still rough and sensitive to the lattice spacing, we anticipate

the more improved lattice calculation to test these predictions.

In addition, we also demonstrated that the axial-vector interaction plays an important role on the $T - \mu_A$ phase diagram of the chirally imbalanced matter. The repulsive (attractive) axial-vector interaction can effectively strengthen (weaken) the chiral phase transition if the coupling is relatively strong. The chiral TCP on the $T - \mu_A$ plane is shifted towards the lower (higher) μ_A region by the repulsive (attractive) axial-vector coupling. This is quite different from (similar to) the role of the vector interaction on the chiral phase transition at finite baryon chemical potential μ .

Since there is no sign problem at finite μ_A , the improved lattice simulation is still very welcome for disclosing the nonperturbative QCD effect on the chiral magnetic effect. Moreover, studying the deviation of the induced current density from the analytic result and locating the TCP in $T - \mu_A$ plane by the lattice simulation can be used to test the instanton molecule picture for $T > T_c$.

We note that if μ_A is introduced by coupling it only to the chiral density, it cannot be considered as a true chemical potential. The reason is that the axial charge is not a conserved quantity due to the axial anomaly. Recently, it is proposed by Robakov [31] that μ_A should be conjugated to a proper combination of the chiral density and a Chern-Simon term, which is a conserved quantity. It is then claimed in [31] that the fact μ_A must be associated with a conserved charge is essential in the discussion for the nonrenormalization of the CME current.

Since there exists a subtlety on the definition of μ_A , a question naturally arises that whether the dynamical axial chemical potential μ'_A defined in this paper can be associated with a conserved charge. We point out that μ'_A does not need to be conjugated to a conserved charge if μ_A could be really well-defined. The reason is that μ'_A is an induced quantity generated dynamically by the axial-vector interaction for nonzero n_A . This is different from the parameter μ_A (assuming it has been well-defined as a true chemical potential), which should be associated with a conserved charge in principle. We note that no matter how μ_A is introduced, it must give rise to nonzero n_A . As demonstrated in this paper, the μ'_A induced by n_A will modify the chiral imbalance described originally by μ_A .

A natural extension of this work is to investigate the role of the axial-vector interaction at finite μ in the presence of an external magnetic field. Conjugate to the induced current for the chiral magnetic effect at finite μ_A , an axial-vector current along the direction of the external magnetic field is generated at finite μ [32]. Another related topic at finite μ is the so called chiral shift parameter [33] in a magnetic field. The roles of the axial-vector interaction in these cases will be reported elsewhere [34].

ACKNOWLEDGMENTS

The author thanks K. Fukushima and N. Yamamoto for useful discussions and helpful comments. This work was supported by the Fundamental Research Funds for the Central Universities of China.

-
- [1] A. A. Belavin, A. M. Polyakov, A. S. Schwartz, and Yu. S. Tyupkin, *Phys. Lett. B* **59**, 85 (1975).
 - [2] E. Witten, *Nucl. Phys. B* **156**, 269 (1979); G. Veneziano, *Nucl. Phys. B* **159**, 213 (1979).
 - [3] D. E. Kharzeev, L. D. McLerran, and H. J. Warringa, *Nucl. Phys. A* **803**, 227 (2008).
 - [4] K. Fukushima, D. E. Kharzeev, and H. J. Warringa, *Phys. Rev. D* **78**, 074033 (2008).
 - [5] L. D. McLerran, E. Mottola, and M. E. Shaposhnikov, *Phys. Rev. D* **43**, 2027 (1991).
 - [6] G. D. Moore, *Phys. Lett. B* **412**, 359 (1997); G. D. Moore and K. Rummukainen, *Phys. Rev. D* **61**, 105008 (2000); D. Bödeker, G. D. Moore, and K. Rummukainen, *Phys. Rev. D* **61**, 056003 (2000); G. D. Moore, [arXiv:hep-ph/0009161](https://arxiv.org/abs/hep-ph/0009161).
 - [7] V. Skokov, A. Y. Illarionov, and V. Toneev, *Int. J. Mod. Phys. A* **24**, 5925 (2009).
 - [8] B. I. Abelev *et al.* (STAR Collaboration), *Phys. Rev. C* **81**, 054908 (2010); *Phys. Rev. Lett.* **103**, 251601 (2009).
 - [9] A. Yamamoto, *Phys. Rev. Lett.* **107**, 031601 (2011).
 - [10] A. Yamamoto, *Phys. Rev. D* **84**, 114504 (2011).
 - [11] T. Schafer and E. V. Shuryak, *Rev. Mod. Phys.* **70**, 323 (1998).
 - [12] E. Ilgenfritz and E. Shuryak, *Nucl. Phys. B* **319**, 511 (1989).
 - [13] E. M. Ilgenfritz and E. V. Shuryak, *Phys. Lett. B* **325**, 263 (1994).
 - [14] T. Schafer, E. V. Shuryak, and J. J. M. Verbaarschot, *Phys. Rev. D* **51**, 1267 (1995).
 - [15] O. Wantz and E. P. S. Shellard, *Nucl. Phys. B* **829**, 110 (2010).
 - [16] G. E. Brown, C.-H. Lee, M. Rho, and E. Shuryak, *Nucl. Phys. A* **740**, 171 (2004).
 - [17] S. Klimt, M. F. M. Lutz, U. Vogl, and W. Weise, *Nucl. Phys. A* **516**, 429 (1990).
 - [18] R. T. Cahill and C. D. Roberts, *Phys. Rev. D* **32**, 2419 (1985).
 - [19] P. C. Tandy, *Prog. Part. Nucl. Phys.* **39**, 117 (1997).
 - [20] Z. Zhang and W.-Q. Zhao, *Phys. Lett. B* **610**, 235 (2005); **612**, 207 (2005); **617**, 157 (2005); Z. Zhang and Y.-x. Liu, *Phys. Rev. C* **75**, 035201 (2007).
 - [21] K. Fukushima, *Phys. Lett. B* **591**, 277 (2004); C. Ratti, M. A. Thaler, and W. Weise, *Phys. Rev. D* **73**, 014019 (2006).

- (2006); S. Roessner, C. Ratti, and W. Weise, *Phys. Rev. D* **75**, 034007 (2007); Z. Zhang and Y.-X. Liu, *Phys. Rev. C* **75**, 064910 (2007).
- [22] K. Fukushima and M. Ruggieri, *Phys. Rev. D* **82**, 054001 (2010).
- [23] K. Fukushima, *Phys. Rev. D* **83**, 111501 (2011).
- [24] H. B. Nielsen and M. Ninomiya, *Phys. Lett. B* **130**, 389 (1983).
- [25] M. Asakawa and K. Yazaki, *Nucl. Phys. A* **504**, 668 (1989).
- [26] K. Fukushima, M. Ruggieri, and R. Gatto, *Phys. Rev. D* **81**, 114031 (2010).
- [27] M. N. Chernodub and A. S. Nedelin, *Phys. Rev. D* **83**, 105008 (2011).
- [28] M. Kitazawa, T. Koide, T. Kunihiro, and Y. Nemoto, *Prog. Theor. Phys.* **108**, 929 (2002).
- [29] Z. Zhang, K. Fukushima, and T. Kunihiro, *Phys. Rev. D* **79**, 014004 (2009); Z. Zhang and T. Kunihiro, *Phys. Rev. D* **80**, 014015 (2009); **83**, 114003 (2011); T. Kunihiro, Y. Minami, and Z. Zhang, *Prog. Theor. Phys. Suppl.* **186**, 447 (2010).
- [30] T. Hatsuda, M. Tachibana, N. Yamamoto, and G. Baym, *Phys. Rev. Lett.* **97**, 122001 (2006); H. Abuki, G. Baym, T. Hatsuda, and N. Yamamoto, *Phys. Rev. D* **81**, 125010 (2010).
- [31] V. A. Rubakov, [arXiv:1005.1888](https://arxiv.org/abs/1005.1888).
- [32] M. A. Metlitski and A. R. Zhitnitsky, *Phys. Rev. D* **72**, 045011 (2005).
- [33] E. V. Gorbar, V. A. Miransky, and I. A. Shovkovy, *Phys. Rev. C* **80**, 032801 (2009).
- [34] Z. Zhang (to be published).